Stresser, M.; Carrasco, R.; Horstmann, J.:

Video-Based Estimation of Surface Currents Using a Low-Cost Quadcopter

In: IEEE Geoscience and Remote Sensing Letters (2017) IEEE

DOI: 10.1109/LGRS.2017.2749120

Video Based Estimation of Surface Currents Using a Low-Cost Quadcopter

Michael Streßer, Ruben Carrasco, and Jochen Horstmann *Member, IEEE*

***Abstract*—Video imagery of surface waves recorded from a small, off the shelf quadcopter with a self-stabilizing camera gimbal is analyzed to estimate the surface current field. The nadir looking camera acquires a short image sequence, which is geocoded to Universal Transverse Mercator (UTM) coordinates. The resulting image sequence is used to quantify characteristic parameters (wave length, period and direction) of short (0.1 to 1 m) surface waves in space and time. This opens the opportunity to fit the linear dispersion relation to the data and thus monitor the frequency shift induced by an ambient current. The fitting is performed by applying a spectral energy based maximization technique in the wavenumber-frequency domain. The current field is compared to measurements acquired by an Acoustic Doppler Current Profiler mounted on a small boat, showing an overall good agreement. The root mean square error in current velocity is 0.09 m/s with no bias.**

***Index Terms*—UAV, surface currents, surface waves, dispersion relation, optical remote sensing, video processing**

I. Introduction

CURRENTS in coastal waters, rivers and estuaries are of high importance for the local environment. They induce forces on structures, mobilize and transport sediments, nutrients, pollutants or heat and induce turbulence. A detailed, high-resolution mapping of the local current field is needed for an efficient and appropriate planning of construction measures as well as to perform a reliable environmental assessment of a certain area. Hence, the flow field is one of the main subjects of hydrographic surveys.

In-situ retrievals of surface flow velocities are commonly carried out by performing a Lagrangian tracking of surface drifters. The lower part of the water column can be observed with Acoustic Doppler Current Profilers (ADCP) in an Eulerian way. Both measurement techniques require extensive vessel operations in order to provide a good spatial coverage and thus both, ADCP and surface drifters, require a tremendous amount of manpower and monetary resources.

Today remote sensing of the current field is typically achieved by using radar based techniques. High-frequency (HF) radar systems have shown to be very useful to measure surface currents [1], [2] with a spatial resolution of ≈ 200 m. Therefore, such systems can be used in coastal applications [3] but in general are not well suited to resolve estuaries or river regions.

Nowadays, the use of marine radars (microwave radars, usually X-Band) to obtain current fields has gained more and more attention [4]. These radars reduce the possible spatial resolution down to approximately 50 m [5], [6]. However, marine radars require the presence of waves that are at least two times longer than the radar ground resolution (typically 7.5 m). This is a major limitation when it comes to an application of marine radar based current retrieval in rivers.

Over the past decade, unmanned aerial vehicles (UAV) have become a widely used tool for optical remote sensing and mapping. However, only a few studies deal with their usage for coastal applications such as bathymetry mapping [7], [8], or beach topographic changes [9].

Within the last five years, position and camera stabilizing performance of commercial multicopters has increased significantly [8] and the cost for these systems have dropped to about 1000 Euro for a complete system.

Within this letter, we demonstrate the applicability of low-cost commercial quadcopters equipped with a self stabilizing camera to retrieve high-resolution surface current maps from image sequences of surface waves. To quantify local currents, we apply a wave dispersion relation fitting technique based on energy maximization in the wavenumber-frequency domain. Similar approaches that are mostly based on least-square fitting techniques have already been applied successfully to marine radar image sequences for a retrieval of wave spectra [10], and surface currents [11], [12] as well as to optical imagery recorded from airplanes for bathymetry and current estimations [13].

II. Equipment and Data

A. Aerial Imagery

The flight platform used within this study is a low-cost, off-the-shelf quadcopter for consumer applications, namely, the DJI Phantom III Professional.

The built-in camera is stabilized with a 3-axis brush-less gimbal, which compensates for yaw, pitch and roll movements of the flight platform. While the camera roll angle is kept at $0°$, the tilt angle is remotely adjustable from $0°$ to $-90°$. For this study, a camera angle of $-90°$ (downward looking) was used. The camera is equipped with a 1/2.3 CMOS sensor with 12.4 megapixels. The manufacturer specifies that the lens has a fix focal length of 20 mm (35 mm format equivalent) and provides a $94°$ field of view (FOV), virtually eliminating unwanted distortion. The video data used for this study were recorded at Ultra-High Definition (3840x2160 pixel) with a frame rate of 25 Hz. By analyzing test videos at different heights, recording a triangle with a known edge length, we found an effective FOV of $76.5°$ and $47.3°$ (horizontal and vertical).

Holman et al. [8] recently studied the station-keeping performance of the Phantom III autopilot. They found that the

UAV is able to keep its position with a standard deviation of 0.20 and 0.53 m (horizontal and vertical) and the viewing angles are correct within standard deviations of 0.25 (tilt and roll) and 0.38 (azimuth). They report a detection of the ground position of imaged objects with 0.21-m accuracy.

Telemetry data are recorded during the entire flight and the initial orientation of the flight platform and the camera are stored in the video meta information.

B. ADCP Measurements

A Teledyne RDI Workhorse 600 MHz ADCP was used to provide ground data of the local flow field. The transducer was mounted $\approx$ 1 m ahead of the bow of a small (7 m) research vessel at a depth of 0.4 m. The vertical cell size was set to 0.25 m and the ensemble integration time was 1.2 s. From the first valid cell which is 0.72 m away from the transducer, five cells are averaged to calculate reliable near surface currents (from 0.72 to 2 m below the surface). It is not possible to measure currents by the ADCP and the Quadcopter at the same time and location. Therefore, the aim of this study is to compare mean river flow velocities. In order to reduce the effect of turbulent fluctuations on the measurements, the ADCP data are down sampled to one velocity vector every 15 m by averaging all ensembles within this distance along the ship track.

C. Experimental Site and Dataset

The study area is located at the Elbe river in Lauenburg, Germany, where the "Elbe-Luebeck-Canal" branches off from the main river. The fortified embankments at the canal entrance form a triangle-shaped peninsula. At the peninsula head the river stream forms a strong shear towards the still water mass in the canal entrance with a continuous recirculation current. The canal has no discharge, except from sporadic weak in- or outflow events when ships are passing the navigational lock a few hundred meters up the canal.

The dataset was acquired at the 4th of April 2017. The ADCP measurements were recorded within 2 h starting $\approx$ 30 minutes after the aerial video recordings.

The video data were acquired at a height of 204 m and 60 seconds of data were used to retrieve the results presented in section IV. The raw video sequence, which shows surface waves propagating throughout the area, is attached to this letter as a media supplement.

III. Methodology

The first step is to assign the video image pixel coordinates given in horizontal (M) and vertical (N) pixel numbers to a rectilinear grid at the water surface (x-axis refers to M, y-axis to N in pixel coordinates). It is generally necessary to remove lens distortion effects like barrel distortion or chromatic abbreviation to perform the geo-rectification. This could be done following the technique described by Holman et al. [8] using the Caltech camera calibration tools (http://www.vision.caltech.edu/bouguetj/calib/doc/). However, the rectilinear lens of the camera shows very little distortion. Nadir looking at a height of 200 m, the errors in pixel size on the ground are < 2.43 cm^2 within the entire camera footprint. Neglecting this small source of error, the pixel dimensions (dx and dy) were considered as constant throughout the whole camera footprint. The imaged area is calculated using the effective FOV of the camera as explained in section II-A.

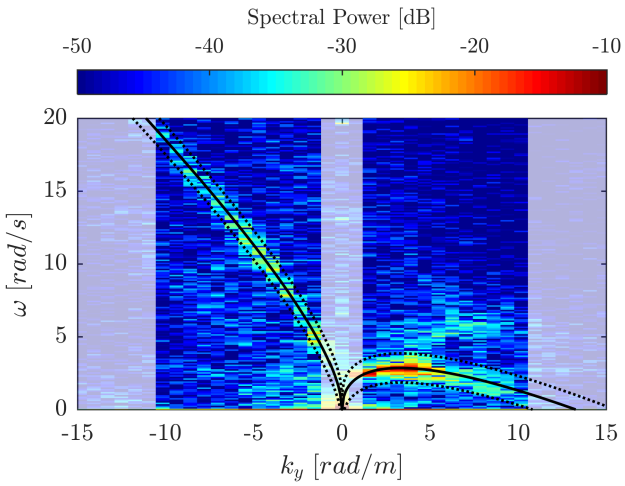

Fig. 1. $k_y - \omega$ plane extracted from an image spectrum. The fitted dispersion curve ($U_y = -0.86$ m/s) is marked as a black line. The filter bandwidth δ of ± 1 rad/s is indicated by the dashed lines.

In the next step the image is divided into a finite number of cells with a specified edge length L_x and L_y. The size of the cells depends on the desired ground resolution but is also restricted by the wave lengths of the imaged waves. For this study we chose a constant window size of 8 by 8 m. Adjacent cells are 50% overlapping which leads to one cell center point every 4 m.

For every cell a gray-scale image sequence is extracted from the video and is converted from the space-time domain to the spectral (wavenumber k_x and k_y and radial frequency ω) domain using a three dimensional Fast-Fourier-Transformation (3D-FFT).

The linear dispersion relation for surface gravity waves in the presence of an ambient current $\mathbf{U}$ reads

$$\omega = \sqrt{g\,|\mathbf{k}|\,tanh(\,|\mathbf{k}|\,d)} + \mathbf{k}\cdot\mathbf{U} \qquad (1)$$

where ω is the radial frequency, $\mathbf{k}$ is the wavenumber vector with components k_x and k_y, d is the water depth and $\mathbf{U}$ is the current vector with components U_x and U_y.

The general idea of dispersion-relation fitting techniques is to separate the spectral power related to surface waves P_w from the power P_n related to the background noise, which is induced by other features. For a known pair of horizontal current components U_x and U_y, the wave related power P_w is defined here as the power within a frequency band of a specified bandwidth δ around the dispersion relation (1). Fig. 1 shows an example spectrum in the k_y-ω-plane. An animation of the full 3D-spectrum is available as a media supplement to this letter. Because the discrete number of spectral bins that are within that bandwidth could vary for different ambient

TABLE I
PROCESSING PARAMETERS

Window size	L_x , L_y	[m]	8
Bandwidth	δ	[rad/s]	1
Low wavenumber cut-off	k_{low}	[rad/m]	1.6
High wavenumber cut-off	k_{high}	[rad/m]	10.7
Minimal current velocity	$u_{x,min}$, $u_{y,min}$	[m/s]	-2.0
Maximal current velocity	$u_{x,max}$, $u_{y,max}$	[m/s]	2.0
Time step	dt	[s]	0.12
Spatial step	dx	[m]	0.083
Spatial step	dy	[m]	0.082

currents, we divide the energy by the number of spectral bins belonging to waves n_w and noise n_n, respectively. Relating both energy density levels we can obtain the signal-to-noise-ratio

$$SNR(U_x, U_y) = \frac{\sum P(k_x,\, k_y,\, \omega)_w}{\sum P(k_x,\, k_y,\, \omega)_n} \frac{n_n}{n_w}. \tag{2}$$

The most likely current speed can be retrieved through a maximization of Eq. 2 for a specified range of possible currents within $U_x \in [u_{x,min}, u_{x,max}]$ and $U_y \in [u_{y,min}, u_{y,max}]$.

To save computing costs, the maximization is done in two runs. For the first run the intervals are discretized with a precision of one decimal place. In a second run, the precision is increased by one decimal place. For the second run the interval ranges for the maximization are limited to the area close (± 0.1m s^{-1}) to the peak, which was found in the first run.

Note that the analyzed wavenumber range is limited to the wavenumbers of interest by introducing a cut-off wavenumber for high and low wavenumbers. Here we limit the wavenumber space from $k_{low} = 1.6$ rad m^{-1} to $k_{high} = 10.7$ rad m^{-1}. According to linear wave theory, the penetration depth of a surface wave is at the order of $(2k)^{-1}$ and the amplitudes of the wave orbital speeds are decaying exponentially with depth. Stewart and Joy [14] proofed that this corresponds to the integrated current from the surface up to this penetration depth. Therefore, the short waves used for the current fit here are expected to be connected to the near surface velocity in the upper decimeters of the water column.

For this high wavenumber regime we can also neglect the influence of water depth on wave dispersion as the hyperbolic tangent converts to unity (e.g. $\tanh(|\mathbf{k}|\, d) > 0.984$ for $k > 1.6$ and $d > 1.5$).

IV. RESULTS

The methodology described in the previous section is applied to the video footage recorded when the quadcopter was hovering for about 60 s at a height of 204 m above the Elbe river. The time step of the video sequence is increased from initially $dt = 0.04$ s (25 frames per second) to $dt = 0.12$ s to decrease computational cost. After geo-referencing, the ground footprint of the video has a width of 322 m and a height of 189 m. The spatial step is found to be $dx = 8.3$ cm and $dy = 8.2$ cm. Table I lists the parameters used for the calculation of the velocity field.

Fig. 2 shows a map of the current velocities acquired by the ADCP (Fig. 2a) and the UAV based current field estimation using the proposed technique (Fig. 2b). In Fig. 2a, the arrows indicate the true locations of the ADCP ensembles, while the color map is interpolated to a regular grid for a better visualization.

The UAV-based current field in Fig. 2b shows a current vector at every second grid cell center while the color map is based on all grid points. Current estimates with a SNR (Eq. 2) smaller than 3 are shown as gray arrows as the wave signal is to weak in that region to perform a reliable current estimation.

It can be seen from Fig. 2, that the UAV-based current field is able to resolve the strong horizontal shear at the border between the fast river stream with speeds around 1 m/s and the still water mass in the canal. Furthermore, also the formation of a recirculation current in the northern part of the area is resolved by both measurement systems.

To compare both systems quantitatively, each ADCP measurement point is compared to an avarage of all UAV-based measurement points that are located less than 5 m away from the particular ADCP measurement. Results are shown as a scatter diagram in Fig. 3. The comparison results in a root-mean-square-error (rmse) of 0.09 m/s without any bias and a correlation of 0.97.

Note that it is not the aim of this study to provide a statistical analysis regarding the performance of the method because the dataset is very limited. Also, this study does not intend to directly compare both measurement systems due to the fact that, on the one hand, it is not possible to perform both measurements exactly at the same time and on the other hand, the video based estimates refer to currents close to the surface whereas the ADCP measuers flow velocities below 0.72 m as mentioned in section II-B. However, the results indicate the capability of the proposed remote sensing technique to acquire a trustworthy estimate of the surface current field. In addition to a vertical profiling by ADCPs, this allows for a more complete record of the local hydrodynamics. Furthermore, it is sometimes not possible to access certain areas by means of survey vessels whereas a remote measurement by air is possible [15].

The video data used within this study have been recorded on a day with covered skies and very low winds ($\approx$ 1.5 m/s). Therefore the waves used for the dispersion relation fitting were small. In these conditions the wind induced surface drift currents as well as the wave induced Stokes-drift is supposed to be small. When these effects increase, a comparison to ADCP data is questionable, because the surface current is not comparable anymore to the near-surface current measured by the ADCP. Hence, future work will focus on studying the impact of the local wave and wind conditions on the UAV-based current estimates as well as the performance of the method in different daylight conditions or sun angles.

The long integration time of 60 s for the UAV-based current field retrieval presented in this study is chosen because this study aims at a comparison to the quasi-steady river flow

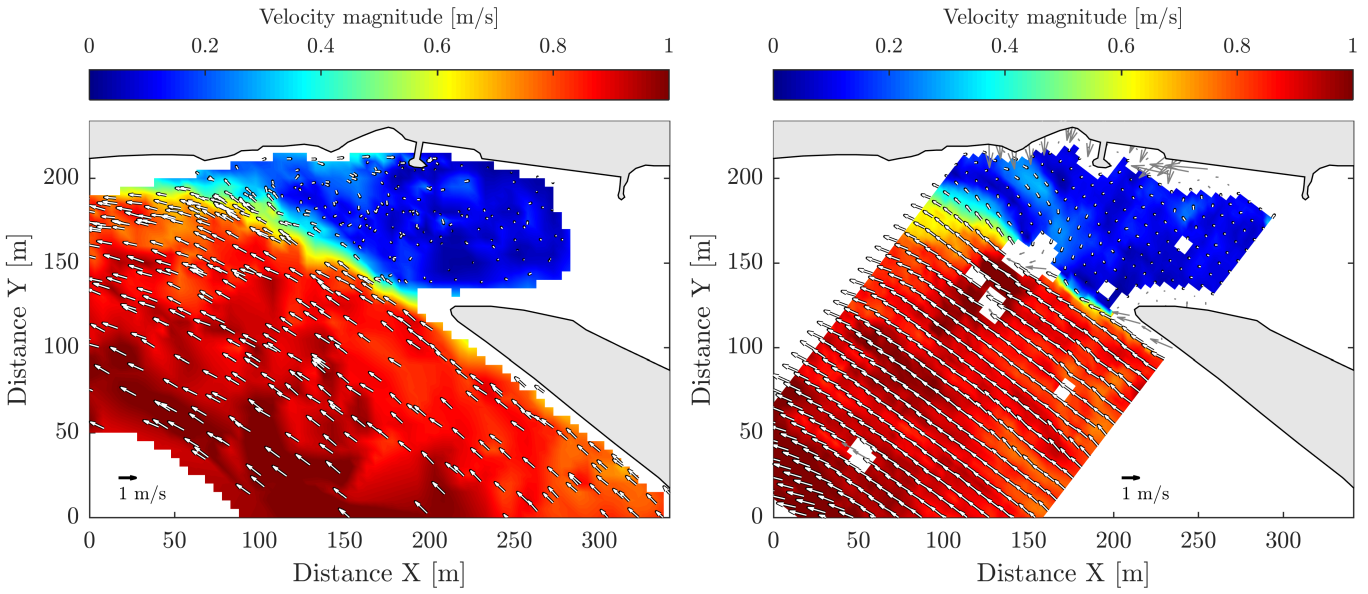

(a) ADCP

(b) UAV

Fig. 2. Current maps acquired from the Acoustic Doppler Current Profiler (ADCP) (a) and estimated from UAV (b) at the Elbe River in Lauenburg. For the ADCP map (a), the current vectors indicate the true locations of the ADCP ensembles and the color coded map is interpolated to a regular grid. The UAV-based current vectors in (b) show every second grid cell center. Low Signal-to-noise ratio areas ($SNR < 3$) are masked and current vectors in these areas are plotted in gray. The origin of the local coordinate system is at 603477 m East and 5914370 m North (UTM32).

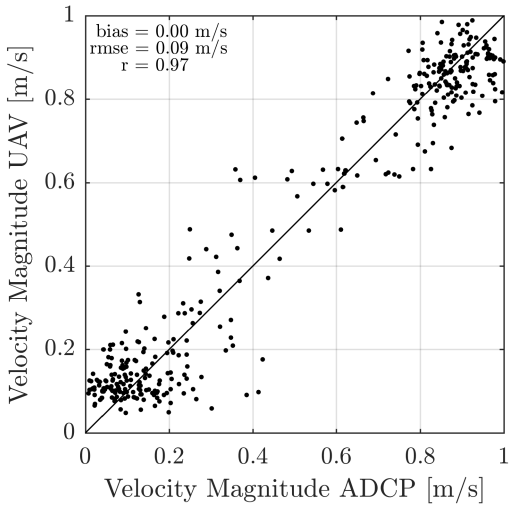

Fig. 3. Scatter diagram of ADCP and UAV-based velocity magnitudes. Only measurements are considered where the ADCP measurement is not more than 5 meters away from the UAV estimate.

field acquired by the ADCP during $\approx$ 1 h. The fact that the local flow shows also a temporal variability during the integration period is also a source of the variability in Fig. 3. Note that in general it possible to decrease the integration time significantly. This allows for acquiring velocity maps with a high variability in space and in time. The highest sampling rate will be strongly dependent on the characteristics of the waves that are visible during the acquisition. A determination of the actual limits of the proposed method is beyond the scope of this letter and will be subject of future studies.

V. Conclusion

In this letter we propose a technique for estimating surface current fields from video sequences recorded from a low-cost, off the shelf quadcopter hovering over a river. After geo-referencing the video data, the estimation is done by fitting the Doppler-shifted surface gravity wave dispersion relation to the three dimensional image spectrum, a widely used approach for marine radar ocean current measurements.

A comparison to ADCP data shows a general applicability (bias = 0.00 m/s, rmse = 0.09 m/s) of the proposed method in low wind and wave conditions with covered skies.

Future work will focus on testing the performance of the technique for different environmental conditions, locations and sun angles.

Acknowledgment

The authors would like to thank Mr. Jan Boedewadt and Mr. Marius Cysewski from Helmholtz-Zentrum-Geesthacht for the acquisition and processing of the ADCP data.

References

[1] J. D. Paduan and L. K. Rosenfeld, "Remotely sensed surface currents in monterey bay from shore-based hf radar (coastal ocean dynamics application radar)," *Journal of Geophysical Research: Oceans*, vol. 101, no. C9, pp. 20 669–20 686, 1996.

[2] K.-W. Gurgel, G. Antonischki, H.-H. Essen, and T. Schlick, "Wellen radar (wera): a new ground-wave {HF} radar for ocean remote sensing," *Coastal Engineering*, vol. 37, no. 34, pp. 219 – 234, 1999.

[3] A. Rubio, J. Mader, L. Corgnati, C. Mantovani, A. Griffa, A. Novellino, C. Quentin, L. Wyatt, J. Schulz-Stellenfleth, J. Horstmann, P. Lorente, E. Zambianchi, M. Hartnett, C. Fernandes, V. Zervakis, P. Gorringe, A. Melet, and I. Puillat, "Hf radar activity in european coastal seas: Next steps toward a pan-european hf radar network," *Frontiers in Marine Science*, vol. 4, p. 8, 2017.

[4] J. Horstmann, J. N. Borge, J. Seemann, R. Carrasco, and B. Lund, *Wind, Wave and Current retrieval utilizing X-Band Marine Radars in Coastal Ocean Observing Systems*. Elsevier, 2015, ch. 16, pp. 281–304.

[5] C. M. Senet, J. Seemann, S. Flampouris, and F. Ziemer, "Determination of bathymetric and current maps by the method disc based on the analysis of nautical x-band radar image sequences of the sea surface (november 2007)," *IEEE Transactions on Geoscience and Remote Sensing*, vol. 46, no. 8, pp. 2267–2279, Aug 2008.

[6] K. Hessner and P. S. Bell, "High resolution current and bathymetry determined by nautical x-band radar in shallow waters," in *OCEANS 2009-EUROPE*, May 2009, pp. 1–5.

[7] R. A. Holman, K. T. Holland, D. M. Lalejini, and S. D. Spansel, "Surf zone characterization from unmanned aerial vehicle imagery," *Ocean Dynamics*, vol. 61, no. 11, pp. 1927–1935, 2011.

[8] R. A. Holman, K. L. Brodie, and N. J. Spore, "Surf zone characterization using a small quadcopter: Technical issues and procedures," *IEEE Transactions on Geoscience and Remote Sensing*, vol. 55, no. 4, pp. 2017–2027, April 2017.

[9] E. Casella, A. Rovere, A. Pedroncini, C. P. Stark, M. Casella, M. Ferrari, and M. Firpo, "Drones as tools for monitoring beach topography changes in the ligurian sea (nw mediterranean)," *Geo-Marine Letters*, vol. 36, no. 2, pp. 151–163, 2016.

[10] I. R. Young, W. Rosenthal, and F. Ziemer, "A three-dimensional analysis of marine radar images for the determination of ocean wave directionality and surface currents," *Journal of Geophysical Research: Oceans*, vol. 90, no. C1, pp. 1049–1059, 1985.

[11] C. M. Senet, J. Seemann, and F. Ziemer, "The near-surface current velocity determined from image sequences of the sea surface," *IEEE Transactions on Geoscience and Remote Sensing*, vol. 39, no. 3, pp. 492–505, Mar 2001.

[12] W. Huang, R. Carrasco, C. Shen, E. W. Gill, and J. Horstmann, "Surface current measurements using x-band marine radar with vertical polarization," *IEEE Transactions on Geoscience and Remote Sensing*, vol. 54, no. 5, pp. 2988–2997, May 2016.

[13] J. P. Dugan, C. C. Piotrowski, and J. Z. Williams, "Water depth and surface current retrievals from airborne optical measurements of surface gravity wave dispersion," *Journal of Geophysical Research: Oceans*, vol. 106, no. C8, pp. 16 903–16 915, 2001.

[14] R. H. Stewart and J. W. Joy, "HF radio measurements of surface currents," *Deep Sea Research and Oceanographic Abstracts*, vol. 21, no. 12, pp. 1039–1049, 1974.

[15] J. Horstmann, M. Stresser, and R. Carrasco, "Surface currents retrieved from airborne video," in *OCEANS 2017 - Aberdeen*, 2017.